RESEARCH ARTICLE | APRIL 01 2024

Conceptual study of a new instrument for dynamic neutron scattering measurements—The modulated intensity with diffraction analysis spectrometer (MIDAS)

Antonio Benedetto ; Gordon J. Kearley ; Antonio Faraone

Rev. Sci. Instrum. 95, 043901 (2024)
https://doi.org/10.1063/5.0193842

Review of Scientific Instruments ARTICLE pubs.aip.org/aip/rsi

Conceptual study of a new instrument for dynamic neutron scattering measurements—The modulated intensity with diffraction analysis spectrometer (MIDAS)

Cite as: Rev. Sci. Instrum. 95, 043901 (2024); doi: 10.1063/5.0193842
Submitted: 23 December 2023 • Accepted: 11 March 2024 •
Published Online: 1 April 2024

Antonio Benedetto,[1,2,3,4,a)] Gordon J. Kearley,[1] and Antonio Faraone[5]

AFFILIATIONS

[1] School of Physics, University College Dublin, Dublin D04 N2E5, Ireland
[2] Conway Institute of Biomolecular and Biomedical Research, University College Dublin, Dublin D04 N2E5, Ireland
[3] Department of Science, University of Roma Tre, 00146 Rome, Italy
[4] Laboratory for Neutron Scattering, Paul Scherrer Institute, 5232 Villigen, Switzerland
[5] Center for Neutron Research, National Institute of Standards and Technology, Gaithersburg, Maryland 20899, USA

[a)] **Author to whom correspondence should be addressed:** antonio.benedetto@ucd.ie

ABSTRACT

Dynamic neutron scattering probes unique nanoscale dynamics via measurement of energy exchanged between a sample and the neutrons. The two spectrometers that investigate processes with characteristic times around a nanosecond are backscattering (BS) and neutron spin-echo (NSE). We present a new method for measuring dynamics using an oscillating cosine-like energy-distribution neutron-package at the sample and measure solely the portion scattered into the elastic line. This portion corresponds to elastically scattered neutrons and, in addition, inelastic components that are scattered with a probability directly proportional to the cosine Fourier-coefficients of the exchanged-energy spectrum. The counts at the detector thus correspond to the van Hove intermediate scattering function. We denote this new method as "Fourier transform neutron scattering" (FTNS), it being broadly analogous to IR and Raman spectroscopies. Here, the realization of such a concept is investigated using an oscillating incident beam produced via a precession method and a secondary spectrometer identical to a BS instrument using crystal analyzers. The instrument is denoted "Modulated Intensity with Diffraction Analysis Spectrometer" (MIDAS). However, simpler approaches, e.g., choppers, may also be used for an FTNS instrument. The theory behind MIDAS is presented, supported by numerical calculations and *in silico* experiments. Finally, we present a Monte Carlo simulation to compare BS and MIDAS spectrometers. This shows that MIDAS has almost 100 times more incident flux than standard BS, but due to the better signal-to-noise ratio of BS, the final information acquisition rate gain of MIDAS is approximately a factor of 2.

I. INTRODUCTION

Dynamic neutron-scattering is a well-established method to investigate motions at the atomic and molecular levels over length scales from a fraction of an angstrom to tens of nanometers and time scales from the picosecond to hundreds of nanoseconds. The research fields range from quantum magnetism, soft matter, to biophysics. Among neutron spectrometers, backscattering (BS) and Neutron Spin-Echo (NSE)[1] possess the highest energy-resolution, providing access to dynamics in the nanosecond range, and are usually employed in the chemical physics, soft-matter, and biophysics communities. BS spectrometers[2] employ crystals to detect (analyze) scattered neutrons of only a specific wavelength, λ_f (for a free neutron, energy and wavelength are simply related by the de Broglie relations; therefore, λ_f corresponds to $E_f = \frac{h^2}{2\lambda_f^2 m_n}$). These spectrometers are optimized for maximum resolution by selecting an angle of reflection of $\approx\pi$ that minimizes the uncertainty of the selected λ_f

from the neutron angle-of-incidence spread. The incoming neutron wavelength, λ_i, and correspondingly, E_i, are scanned using either crystal monochromators or Time-of-Flight (ToF) methods. Thus, they operate in the energy domain, measuring the probability distribution, within a certain solid angle, of the neutron-energy exchange, $\Delta E = E_f - E_i$, due to the scattering by the sample, which is proportional to the dynamic structure-factor, $S(Q, \Delta E)$, where Q, the wavevector transfer, defines the length scale probed. NSE[3] spectrometers are unique because they employ the neutron-spin as an internal clock to time the neutron passage in the first and second arms of the spectrometer. Thus, they measure small differences in the energy of the neutron before and after interaction with the sample. Hence, poorly monochromatized beams can be employed, with significant gains in flux, without sacrificing energy resolution, which can reach values of ≈1 neV, corresponding to a longest time scale of ≈1 μs. This resolution enables the study of processes over time scales of several hundred nanoseconds. NSE works in the time domain, providing the normalized Intermediate Scattering Function (ISF), I(Q, t)/I(Q, 0), directly. This is simply the Fourier transform of the dynamic structure factor.

Among BS spectrometers, those operating at continuous sources, such as IN16B at the Institute Laue–Langevin (ILL),[4–7] SPHERES at the Maier–Leibnitz Zentrum (MLZ),[8] EMU of the Australian Nuclear Science and Technology Organisation (ANSTO),[9] or HFBS[10] at the National Institute of Standards and Technology (NIST) Center for Neutron Research (NCNR), reach the highest energy resolutions. They employ strained or polished Si (111) crystals, providing energy resolutions of ≈1 and ≈0.3 μeV, respectively. Even higher energy resolutions, ≈0.08 μeV and theoretically ≈0.02 μeV, are accessible using, for example, GaAs (200) analyzers, with, however, significant losses in data acquisition rates.[11] During a measurement, the incoming energy is defined using a monochromator consisting of the same type of crystal as the analyzer; the incoming energy is continuously scanned, most commonly using a Doppler drive at present.[7] This mode of operation is inefficient for scanning large dynamic-windows, although mixed ToF backscattering operation modes are also successfully employed.[5] The limitations on the dynamic window are best overcome with backscattering instruments at pulsed sources.[12–14] These instruments define the final energy of the neutrons using similar crystal analyzers to those described above, whereas the incoming energy is determined by the neutron time-of-flight. However, to optimize the instrument, energy resolution needs to be sacrificed and these spectrometers operate most commonly in quasi-backscattering mode with an energy resolution of ≈3 μeV (or worse if higher fluxes are preferred[15]).

NSE spectrometers require an exquisite (of the order of few parts per million) control of the magnetic field experienced by the neutrons, which limits the size of the detector coverage. To overcome this, anti-Helmholtz coils are used, which were first employed on SPAN at the HMI[16,17] and recently implemented on WASP[18] at ILL (EXPANSE,[19] an instrument similar to WASP is being developed for the second target station at the SNS, ORNL). In this way, a detector coverage of almost 360° in the scattering plane is achievable. Nevertheless, the maximum time accessible is severely reduced compared to state of the art[20–22] NSEs (by a factor ≈4), reaching times of ≈10 ns when incoming neutrons with a similar wavelength as those selected using a Si (111) crystal, 6.2708 Å, are employed. Moreover, the vertical acceptance is still limited (2.5° for WASP), whereas backscattering spectrometers have an analyzer coverage of $\approx\pi$ steradian. Nevertheless, the flux on the sample of a NSE spectrometer is more than 100 times that of a high resolution (1 μeV or better) BS spectrometer, and it is a very flexible instrument in terms of the dynamic range covered. On the other hand, incoherent scattering has a 2/3 probability of flipping the neutron spin, resulting, as it will be discussed later, in a degradation of the beam polarization and an inherent reduction in the signal-to-noise ratio. Although NSE spectrometers do not require a pulsed beam (but they can operate at spallation sources[23] in ToF mode[24]), they, nevertheless, measure the ISF single value of t (called Fourier time) at a time.

BS spectrometers are employed to perform both Inelastic and Quasielastic Neutron Scattering (INS and QENS) measurements, investigating oscillatory dynamics, such as vibrations, and relaxational processes, such as diffusion. NSE spectrometers, with a few notable exceptions,[25] are used to study relaxational processes. Non-energy-resolved NSE instruments can employ Larmor diffraction to study, for example, structural effects related to magnetic ordering[26] or use the principles of neutron spin echo to encode the scattering angle of the neutron to obtain structural information over large length scales.[27,28] Moreover, variation of the classical NSE setup, such as the neutron spectral modulation setup,[29] or the use of Resonance NSE (RNSE)[26] has been proposed to measure excitations and magnetic scattering. Logically, vibrations, which are characterized by a specific frequency, are conveniently investigated in the energy domain, and relaxational processes are more conveniently measured in the time domain. In fact, in the absence of modeling, in the energy domain, it is hard to discern qualitative features of the dynamics, such as multimodality, which are characterized by broad distributions of relaxation processes.

Modern BS spectrometers reach a signal-to-noise ratio of 10^5, measured as the ratio between the peak intensity and the background level of the spectra for an elastic sample (resolution).[4] This characteristic is essential for the ability to detect small inelastic contributions but is less important for the measurement of the broadening of the QENS signal. For NSE spectrometers, the signal-to-noise ratio could be defined as the ratio between the echo amplitude and the average echo value. This, in turn, depends on the beam polarization. Using modern polarizers, polarization values larger than 0.95 can be achieved. However, a partial depolarization of the scattered beam takes place because of the presence of incoherent scattering from the sample. This translates to values of the amplitude over the average of the echo value of the order of $(1 + P_s)/2$, where P_s is the polarization of the scattered beam. For a purely coherent sample, $P_s = 1$, whereas for a purely incoherent sample $P_s = -1/3$. Such a limitation in the signal-to-noise ratio is common to all Fourier methods, such as NSE, which is compensated by the possibility to use a broad incoming neutron distribution, and hence a high detection rate, retaining a high resolution.

A successful and efficient way of operating BS spectrometers at continuous sources is the "elastic scan."[30–32] In this mode, the spectrometer is set to only detect neutrons in the elastic channel, i.e., which have exchanged no energy with the sample within the instrumental resolution-limit. An external parameter is then scanned, usually the sample temperature. Because of the high count

rate, it only takes a few hours to recognize the onset of nanosecond dynamics in the sample. However, since the dynamic structure factor is not determined, detailed information is difficult to extract.

Recently, some of us proposed a new dynamic neutron-scattering method, van Hove Integral (vHI), which measures the running-time integral of the ISF, which we denoted as vHI profile. vHI is an elastic scattering method in which the bandwidth of the incoming neutron beam (effectively the instrument resolution) is varied and the elastically scattered neutrons are selected using a fixed analyzer window. This method offers the advantage of measuring the system dynamics directly in the time domain and has a high count-rate because the integrated elastic-scattering is always measured.[33–36]

The current paper can be regarded as a modification to the vHI method employing an incident beam periodically modulated in λ_i. This gives us access directly to the ISF, rather than its running integral (as in vHI). In particular, we will discuss an instrument where the modulated beam was achieved using precession methods similar to modulated intensity NSE,[37,38] whereas the secondary spectrometer is the same as a high resolution BS spectrometer. This covers time scales in the nanosecond range. In the remainder of this paper, we will use a convenient acronym for an instrument using this concept: MIDAS (Modulated Intensity with Diffraction Analysis Spectrometer). This arrangement gives the detector solid-angle advantage of a BS machine for the secondary spectrometer and broadens the dynamic window to reach time scales as fast as few picoseconds. Moreover, this method has the potential advantage of providing multiplexing opportunities to achieve an improved count-rate. On the negative side, however, the primary beam must be polarized (50% loss) and, because there is no echo, the refocusing advantage of NSE is lost. It is also difficult to match the very low background and high signal-to-noise ratio achieved using BS instruments.

For completeness, we mention here that the use of an analyzer crystal on a NSE instrument was envisaged early on by Mezei and coworkers for the investigation of inelastic peaks. Such a concept was employed at the now decommissioned spin echo spectrometer IN11 at the ILL.[39] However, the use of crystal analyzers in conjunction with precession methods to broaden the scattering angle coverage and as an alternative to the echo decoding was not suggested before, to the best of our knowledge.

This paper is set out in four sections as follows: Section II deals with the theoretical aspects of the instrument, proving that the principle is sound. In Sec. III, we take a more numerical approach to the instrument to demonstrate more clearly how the instrument functions and its dynamic range. A test experiment or Monte Carlo simulation that would enable us to position MIDAS relative to existing spectrometers, such as IN16B and WASP, is well beyond the scope of this paper. However, in Sec. IV, we establish that the MIDAS concept is worthwhile by presenting a Monte Carlo (McStas[40,41]) simulation of the instrument and compare this with an equivalent BS instrument in order to gauge the potential advantages of MIDAS. Finally, in Sec. V, we will conclude discussing merits and disadvantages of MIDAS in comparison with other methods and instruments.

II. THEORETICAL FRAMEWORK

Figure 1 shows a synoptic comparison among BS, vHI, and MIDAS spectrometers. They all use the same secondary spectrometer. Crystal analyzers surrounding the sample are aligned to reflect neutrons of appropriate wavelength, λ_f, back through the sample, reaching the detectors that are located behind the sample. The low scattering-probability of the sample ensures that although neutrons go through the sample twice, the detected intensity is not significantly reduced. A duty cycle is provided using an appropriate chopper, e.g., in the shape of a trifoil, and the events at the detector are discriminated in time to differentiate between the neutrons scattered by the sample directly to the detector from those that have been reflected by the analyzer. The three instruments differ in the wavelength distribution of the incoming beam, $\rho_1(\lambda)$. ρ_1 is described by a set of instrumental parameters, $\{P_i\}$. The scattered-beam wavelength-distribution, ρ_2, is determined by the convolution of the incoming beam with the sample dynamic structure-factor,

$$\rho_2(\{P_i\}, E, S) = \rho_1 \otimes S = I_0 \int_{-\infty}^{\infty} \rho_1\left(\{P_i\}, E - E'\right) S\left(Q, E'\right) dE', \quad (1)$$

where I_0 indicates the incoming flux.

The analyzer operates as a filter function, $F(\{P_f\}, E)$, mainly characterized by the energy of the reflected neutrons, E_f, and by its uncertainty, dE_f. The neutrons detected are given by

$$N_d\left(\{P_i\}, \{P_f\}, S\right) = \int_{-\infty}^{\infty} \rho_2(\{P_i\}, E, S) F\left(\{P_f\}, E\right) dE. \quad (2)$$

The instrumental energy resolution-function can be defined as the response of the instrument when the dynamic structure-factor is a Dirac delta function, $\delta(E)$,

$$N_d\left(\{P_i\}, \{P_f\}, S = \delta\left(E'\right)\right) = R\left(\{P_i\}, \{P_f\}\right) = I_0 \int_{-\infty}^{\infty} \rho_1 \times (\{P_i\}, E) F\left(\{P_f\}, E\right) dE. \quad (3)$$

For simplicity, we will restrict our discussion to the case of BS spectrometers at continuous sources because they have the highest energy-resolution. The incoming wavelength-distribution is defined using a Neutron Velocity-Selector (NVS). This element reduces the background and eliminates higher-order reflection components. As mentioned above, BS spectrometers at continuous sources normally use monochromators with the same characteristics as the analyzers in the secondary spectrometer. To scan the energy, the incoming wavelength is varied, for example, by changing the d-spacing of the monochromator crystal by scanning the temperature, as on IN13 at ILL,[42,43] or more commonly by placing the monochromator on a moving drive, resulting in a varying E_i, due to the Doppler effect.[7,10] On the other hand, the energy spread of the filter function remains constant as E_i is scanned. We model ρ_1 and F as Gaussian functions centered at E_i and E_f, respectively, with standard deviations dE_i and dE_f, respectively. This description is sufficiently accurate for the present purpose and quite realistic for BS at continuous sources. Nevertheless, it is possible that more complex functional forms are required to describe the instrumental resolution-function,

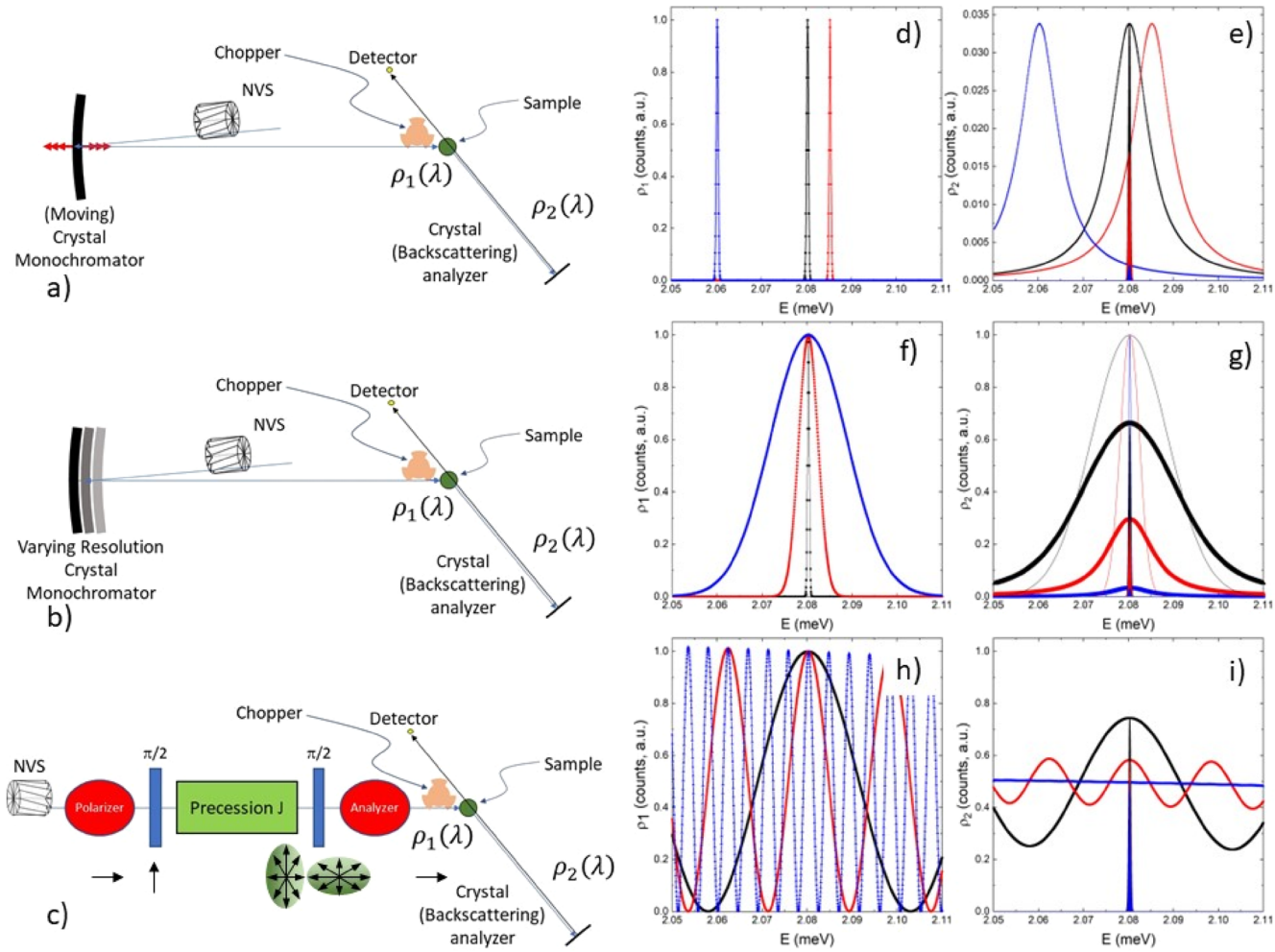

FIG. 1. (a)–(c) Diagrams showing the layout and operation of BS, vHI, and FTNS spectrometers, respectively. (d), (f), and (h) Wavelength distribution of the incoming neutron beam for three instrument configurations, for BS, vHI, and FTNS spectrometers with Si (111) crystal analyzers, respectively. (e), (g), and (i) Wavelength distribution of the scattered neutron beam, for BS, vHI, and FTNS spectrometers, respectively; the shaded areas around $E = 2.0803$ meV represent the neutrons selected using the analyzers, which reach the detector.

as, for example, is well known for BS without a pulse shaping chopper at spallation sources. Using Eq. (2), it is easy to demonstrate that the instrument resolution-function is a Gaussian with standard deviation given by the square average of dE_i and dE_f, i.e., the convolution of ρ_1 and F. Similarly, Eqs. (1)–(3) indicate that the result of a measurement scanning ΔE is the convolution of $S(Q, \Delta E)$ and the instrument energy resolution function.

The theory and equations of vHI have recently been reported by some of us.[33–36]

In MIDAS, the primary spectrometer is the same as a modulated intensity NSE.[38] As in NSE spectrometers, the NVS defines the Q-resolution and ensures that elements, such as the π flippers, whose operation depends on the neutron wavelength, operate in an appropriate range. With reference to Fig. 1(c), the beam is polarized along the beam path, using a transmission polarizer, usually a V-cavity, and a $\pi/2$ flipper rotates the beam polarization to the transverse direction. The neutron beam then enters a longitudinal magnetic-field in which the precession of the spins begins. Because of the polychromaticity of the beam, the neutrons spend different times in the magnetic field, and by the end of the precession area, the beam is fully depolarized, with all possible directions in the transverse plane being equally probable. A second $\pi/2$ flipper then projects the beam polarization in the scattering plane. The neutron polarization is analyzed using a device that needs to be compact and could be a ^{3}He cell or a supermirror, such as a bender.[44–46] This device allows neutrons to be transmitted with a probability proportional to the cosine

of the angle between the spin direction and the longitudinal direction. Thus, the energy distribution of the incoming beam is defined as

$$\rho_1(J,\phi_0,E) = \frac{1}{2}\left[1+\cos\left(\gamma\sqrt{\frac{m_n}{2}}\frac{J}{\sqrt{E}}+\phi_0\right)\right], \tag{4}$$

where γ is the gyromagnetic ratio. The incoming beam is defined in terms of the following parameters: J, the field integral of the magnetic field experienced by the neutrons, $J = \int Bdl$, along their path and a phase parameter, and ϕ_0, which can be controlled by the operation of the π/2 flippers. The incoming wavelength modulation from the NVS is much broader than the range of energies of interest, and therefore, this contribution has been neglected here.

Naturally, as in other Modulation of Intensity Emerging from Zero Effort (MIEZE) instruments, the polarization encoding could also be performed using resonance flippers.[47,48]

Substituting Eq. (4) into Eq. (1), we rewrite Eq. (2) as

$$N_d(J,\phi_0,E_f,dE_f,S) =$$

$$I_0\int_{-\infty}^{\infty}\left\{\int_{-\infty}^{\infty}\frac{1}{2}\left[1+\cos\left(\gamma\sqrt{\frac{m_n}{2}}\frac{J}{\sqrt{E-E'}}+\phi_0\right)\right]S(Q,E')dE'\right\} \times F(E_f,dE_f,E)dE. \tag{5}$$

Within the approximation that the filter function of the analyzer is very narrow compared to the period of the oscillation of the incoming wavelength distribution at around E_f, we make the following approximation:

$$F(E_f,dE_f,E) = \delta(E-E_f). \tag{6}$$

Equation (5) becomes

$$N_d(J,\phi_0,E_f,dE_f\approx 0,S) \approx I_0\int_{-\infty}^{\infty}\left\{\int_{-\infty}^{\infty}\frac{1}{2}\left[1+\cos\left(\gamma\sqrt{\frac{m_n}{2}}\frac{J}{\sqrt{E-E'}}+\phi_0\right)\right]S(Q,E')dE'\right\}\delta \times (E-E_f)dE = I_0\int_{-\infty}^{\infty}\frac{1}{2}\left[1+\cos\left(\gamma\sqrt{\frac{m_n}{2}}\frac{J}{\sqrt{E_f-E}}+\phi_0\right)\right] \times S(Q,E)dE. \tag{7}$$

We can perform a series expansion around $E = E_f$, taking advantage of the fact that for $\frac{E}{E_f} \ll 1$,

$$\left(1-\frac{E}{E_f}\right)^{-1/2} \approx 1+\frac{1}{2}\frac{E}{E_f}, \tag{8}$$

to obtain

$$N_d(J,\phi_0,E_f,dE_f\approx 0,S) \approx I_0\int_{-\infty}^{\infty}\frac{1}{2}\left[1+\cos\left(\gamma\sqrt{\frac{m_n}{2}}\frac{J}{\sqrt{E_f}}+\frac{t_F E}{\hbar}+\phi_0\right)\right]S(Q,E)dE, \tag{9}$$

where we define the Fourier time as

$$t_F = \frac{1}{2E_f}\frac{1}{\sqrt{2E_f}}\gamma\sqrt{m_n}\hbar J = \gamma m_n^2\frac{1}{2\pi h^2}\lambda_f^3 J. \tag{10}$$

Equation (10) highlights the well-known dependence of the Fourier time from the third power of wavelength, in this case the final wavelength selected using the crystal analyzer, λ_f.

Equation (9) reduces to

$$N_d(J,\phi_0,E_f,dE_f\approx 0,S) \approx I_0\int_{-\infty}^{\infty}\frac{1}{2}\left[1+\cos\left(\frac{t_F E}{\hbar}\right)\right]S(Q,E)dE \tag{11}$$

by setting the π/2 flippers such that

$$\phi_0+\gamma\sqrt{\frac{m_n}{2E_f}}J = 2n\pi, \tag{12}$$

or, with $\phi_0 = 0$, choosing J such that

$$\gamma\sqrt{\frac{m_n}{2E_f}}J = 2n\pi. \tag{13}$$

As commonly done in NSE spectrometers, this latter condition can be easily achieved adding within the precession coil, which creates the precession field, a smaller phase coil to fine-tune the field integral experienced by the neutrons.

It is clear that

$$\int_{-\infty}^{\infty}\cos\left(\frac{t_F E}{\hbar}\right)S(Q,E)dE = \hbar\int_{-\infty}^{\infty}\cos(\omega t_F)S(Q,\omega)d\omega = \hbar I(Q,t_F), \tag{14}$$

$$\int_{-\infty}^{\infty}S(Q,E)dE = \hbar S(Q) = \hbar I(Q,t_F=0) = \hbar I(Q,0). \tag{15}$$

Therefore, in conclusion, within the constraints outlined above, the detected signal is independent of the energy selected using the analyzer and corresponds to a measurement of the sum of the static structure-factor and the ISF. The value of the field integral defines (in combination with the value of E_f) the Fourier time and the time scale at which the sample dynamics is probed,

$$N_d(J) \approx \frac{1}{2}\hbar I_0[I(Q,0)+I(Q,t_F)]. \tag{16}$$

Turning the π/2 flippers off results in an incoming beam without wavelength modulation, which can be used for normalization purposes,

$$N_d^{off} \approx \hbar I_0[I(Q,0)], \tag{17}$$

$$\frac{I(Q,t_F)}{I(Q,0)} = 2\frac{N_d(J)}{N_d^{off}}-1. \tag{18}$$

Alternatively, the π/2 flippers could be set such that

$$\phi_0+\gamma\sqrt{\frac{m_n}{2E_f}}J = (2n+1)\pi, \tag{19}$$

or, with $\phi_0 = 0$, the phase field could be chosen such that

$$\gamma\sqrt{\frac{m_n}{2E_f}}J = (2n+1)\pi, \tag{20}$$

resulting in

$$N_d\left(J,\phi_0,E_f,dE_f\approx 0,S\right)\approx I_0\int_{-\infty}^{\infty}\frac{1}{2}\left[1-\cos\left(\frac{t_F E}{\hbar}\right)\right]S(Q,E)dE \tag{21}$$

and

$$\frac{I(Q,t_F)}{I(Q,0)}=1-2\frac{N_d(J)}{N_d^{off}}. \tag{22}$$

The expert reader will not be surprised by the results of Eqs. (18) and (22) and will recognize the close similarities between the argument above and the well-established theory of NSE and similar methods, such as RNSE or MIEZE.[48,49] As in MIEZE, for example, scattering from the sample has the effect of smearing the incoming beam modulations;[47] the job of the analyzer is to measure the detected intensity at a specific point to determine the modulations. In MIEZE, the modulation itself is measured as a function of time; in MIDAS, only one point is detected because the beam is not pulsed.[47] We will discuss later how it is possible to measure more than one point in the modulation profile to improve the measuring efficiency.

In Sec. III, numerical calculations will be carried out to establish the boundaries of applicability of this framework.

III. NUMERICALLY CALCULATED RESULTS

In this section, we will give an overview of the operational range of MIDAS by calculating its performance numerically in order to validate the approximations used above. The calculations were performed using MATLAB. First, the incoming wavelength-distribution was defined by a Gaussian function to mimic the presence of the NVS. NSE spectrometers commonly operate with a $\Delta\lambda/\lambda$ between 10% and 20%. Then, the modulation of intensity due to the polarizer–$\pi/2$ flipper (precession)—$\pi/2$ flipper (polarization) analyzer system was calculated to define $\rho_1(\lambda)$ as a function of λ, with equally spaced points. The distribution was then converted to equally spaced energy-bins using the "resample" algorithm in MATLAB, ensuring that correct account was taken for the conversion in bin width from wavelength to energy. $\rho_1(E)$ was subsequently convoluted with the dynamic structure-factor using the "conv" algorithm in MATLAB. This provided ρ_2(E), which was multiplied by the filter function $F(E)$ and the resulting distribution integrated using a trapezoidal algorithm, "trapz," in MATLAB. The crystal-analyzer filter-function $F(E)$ was modeled as a Gaussian function.

To explore the dynamic range potentially available to MIDAS, we will compare results using three types of crystal analyzers, namely strained Si (111), polished Si (111), and GaAs (200). These are all currently used on IN16B. We estimate the Full Width at Half Maximum (FWHM) of the filter function from the reported instrumental resolution dividing by a factor of $\sqrt{2}$. Clearly, the exact value is of little importance for the current discussion. For strained Si (111), polished Si (111), and GaAs (200), we use a FWHM of 0.60, 0.20, and 0.05 μeV, respectively.

The minimum value of the field integral, J, is limited because a minimum guide field larger than the earth magnetic field is necessary so that neutrons retain their polarization. Possibilities to further reduce this field integral are, however, available. These use appropriate π flippers to obtain an effective field-integral from the difference between the field integrals experienced by the neutrons along an appropriately defined path. This option has been developed for the NSE at the SNS, ORNL.[23] For our calculations, we will use a minimum J of 10^{-4} Tm.

As mentioned above, the instrumental resolution of a NSE spectrometer is determined by its capability to maintain the field-integral inhomogeneities within few ppm. Slight differences in the field integral along the neutron path slightly shift the phase of the echo signal with a resulting reduction in the modulations, which is due to the instrument. This aspect will be discussed in detail later. State of the art NSE reaches maximum field integrals of the order of 1 Tm, maintaining visibility of the echo, using a combination of optimally designed precession fields and radial correction coils. At $\lambda_f \approx 6$ Å, a field integral of 1 Tm would correspond to a resolution with a FWHM of ≈25 neV. However, in MIDAS, the practical limitations on the maximum required field-integral are somewhat lower, being set by the width of the crystal-analyzer filter function. The results of MIDAS need to be corrected for effective resolution by dividing for the response of a resolution sample, as is common practice in QENS spectrometers. This was operatively done by setting $\rho_2(E)=\rho_1(E)$. Note, however, that MIDAS (as NSE and vHI) has the advantage that the instrumental response function, the resolution, can be simply divided out. This is a clear advantage over instruments that measure in the energy domain, which requires some deconvolution procedure to account for instrumental resolution. Therefore, the normalized ISF was obtained by

$$\frac{I(Q,t_F)}{I(Q,0)}=\frac{2\frac{N_d^s(J)}{N_d^{s,off}}-1}{2\frac{N_d^R(J)}{N_d^{R,off}}-1}, \tag{23}$$

where the superscripts s and R indicate whether the counts have been taken on the sample or the resolution.

Figure 2 shows the results of the calculated response of MIDAS for samples having dynamic structure-factors modeled as Lorentzian functions,

$$S(Q,\Delta E)=\frac{1}{2\pi}\frac{\Gamma}{\Delta E^2+\left(\frac{\Gamma}{2}\right)^2}, \tag{24}$$

with various FWHM, Γ, in the range from 0.1 meV to 0.01 μeV, covering four orders of magnitude.

The results for three possible types of analyzers are compared. In the three plots, the thick black continuous lines represent the resolution function for the three types of analyzers. This function would be experimentally obtained by measuring a sample that has no dynamics in the energy range probed, typically vanadium. The open data points represent the results calculated by simply estimating the counts at the detector and employing Eq. (18). The solid data points are corrected for the instrumental resolution-function.

The resolution starts deviating from 1 at values of J such that $\gamma\sqrt{\frac{m_n}{2}}\frac{J}{2Ef\sqrt{Ef}}dE_f \approx 5\%\ of\ 2\pi$. Remarkably, however, the results of the measurement after correction for the resolution function are still in excellent agreement with the expected results. In practice, this does not imply that measurements are possible even when the resolution function drops significantly because the counting uncertainty

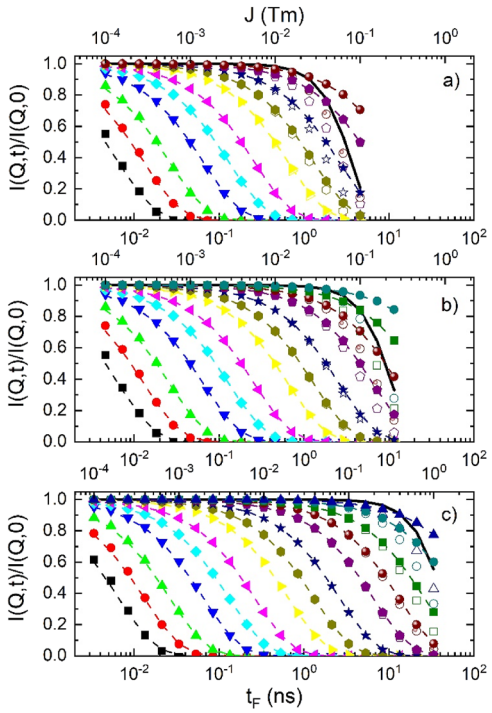

FIG. 2. Normalized ISF calculated as the response of MIDAS for Lorentzian dynamic structure-factors with various values of FWHM: black 0.2 meV, red 0.1 meV, green 0.05 meV, blue 0.02 meV, cyan 0.01 meV, magenta 5 μeV, yellow 2 μeV, dark yellow 1 μeV, navy 0.5 μeV, purple 0.2 μeV, wine 0.1 μeV, olive 0.05 μeV, dark cyan 0.02 μeV, and royal 0.01 μeV. Plots (a)–(c) refer to crystal analyzers with resolutions (FWHM) of 0.6 μeV [strained Si (111)], 0.2 μeV [polished Si (111)], and 0.05 μeV [GaAs (200)], respectively. In all cases, $\Delta\lambda/\lambda$ defined using the NVS was 0.2. Solid black lines represent the instrumental resolution; solid symbols represent the normalized ISF calculated after resolution correction using Eq. (23); open symbols represent the normalized ISF calculated without resolution correction using Eq. (18); and dashed lines represent the exponential decays corresponding to the analytical Fourier-transform of the Lorentzian dynamic structure-factors.

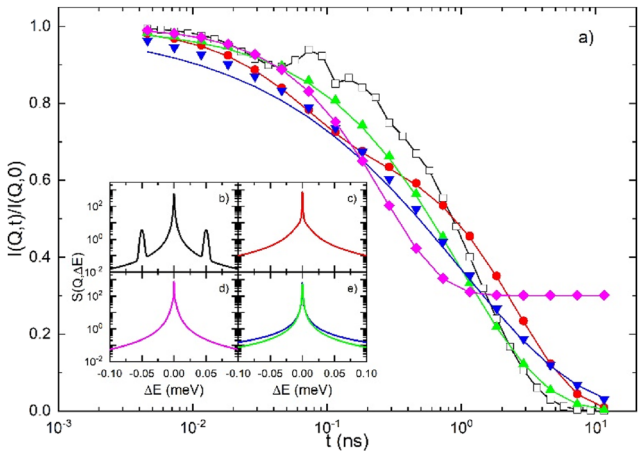

FIG. 3. (a) Normalized ISF calculated as the response of MIDAS as detailed in the text. Open black squares: sum of one Lorentzian of FWHM 1 μeV and two inelastic Gaussian peaks centered at $\pm$50 μeV and FWHM 5 μeV (plot b); red circles: sum of two Lorentzians of FWHM 20 and 0.5 μeV and normalized areas of 0.3 and 0.7, respectively (plot c); magenta diamonds: sum of a Lorentzian of FWHM 5 μeV and a delta function with normalized areas of 0.7 and 0.3, respectively (plot d); and triangles: Fourier transform of a stretched exponential function with characteristic time 1 ns and stretching exponent 0.7 (green) and 0.5 (blue) (plot e). The continuous lines represent the corresponding analytical normalized ISFs. Please note that in plot (b)–(e), the dynamic structure factor is convoluted with a Gaussian resolution function with FWHM 0.28 μeV.

will result in unreliable results; typically, values of the resolution below 1/e are prohibitive. However, this result does show that systematic errors introduced by the finite wavelength-spread of the analyzed beam can be corrected.

In the short-time limit, for FWHM of the order of 100 μeV and broader, there is some small but appreciable difference between the calculated response and the analytical expectation. We will discuss this point in more detail below.

In general, the agreement between the calculated and analytically expected results is very good, certainly within the range of uncertainty of typical dynamic neutron-scattering experiments, which are of the order of few percent. Therefore, the approximation employed in the theoretical derivations of Sec. II is realistic at least within the range tested.

Figure 3 shows the calculated response of MIDAS for different, commonly encountered, line shapes of the dynamic structure factor. The cases considered are the sum of one Lorentzian and two inelastic Gaussian peaks [Eq. (25)], the sum of two Lorentzian functions [Eq. (26)], the sum of a Lorentzian and delta function [Eq. (27)], and the Fourier transform of a stretched exponential [Eq. (28)] and are expressed as follows:

$$S(Q,\Delta E) = f\frac{1}{\pi}\frac{\frac{\Gamma}{2}}{\Delta E^2 + \left(\frac{\Gamma}{2}\right)^2} + (1-f)\left\{\frac{1}{\sigma\sqrt{2\pi}}\left[e^{\frac{-(\Delta E - E_{ins})^2}{2\sigma^2}} + e^{\frac{-(\Delta E + E_{ins})^2}{2\sigma^2}}\right]\right\}, \quad (25)$$

$$S(Q,\Delta E) = f\frac{1}{\pi}\frac{\frac{\Gamma_1}{2}}{\Delta E^2 + \left(\frac{\Gamma_1}{2}\right)^2} + (1-f)\frac{1}{\pi}\frac{\frac{\Gamma_2}{2}}{\Delta E^2 + \left(\frac{\Gamma_2}{2}\right)^2}, \quad (26)$$

$$S(Q,\Delta E) = f\frac{1}{\pi}\frac{\frac{\Gamma}{2}}{\Delta E^2 + \left(\frac{\Gamma}{2}\right)^2} + (1-f)\delta(\Delta E), \quad (27)$$

$$S(Q,\Delta E) = F\left\{\exp\left[-\left(\frac{t}{\tau}\right)^{\beta}\right]\right\}. \quad (28)$$

The presence of inelastic features in the μeV region is common for tunneling phenomena that frequently arise from transitions between the quantum-rotational splitting of the librational ground-state of rotors, such as CH_3 and NH_3 groups, or molecular ions, such as NH_4^+ and BH_4^+.[50] These measurements provide a precise value of the magnitude and form of the rotational potential, which has been of interest at a fundamental level and in the evaluation of the rotational potential for molecular-dynamics simulations. The peak

position and its intensity as a function of Q are both of importance in this type of work. QENS spectra are routinely analyzed in terms of summation of two or more Lorentzian functions. Such a line shape is expected, for example, if more than one population of scatterers with different dynamics is present. Moreover, rotational motions are described by sums of Lorentzians with different weights and widths.[51] Furthermore, the presence of a delta function, a resolution limited peak, in the energy spectra indicates immobile scatterers or scatterers that can return to their original position, either because they are confined or because they can only perform motions such as rotations with respect to a fixed point (within the experimental time scale).

The stretched exponential function, $\exp\left[-\left(\frac{t}{\tau}\right)^{\beta}\right]$, is a phenomenological expression that is often used to describe non-Debye relaxation processes. In the limit of the stretching exponent $\beta = 1$, an exponential relaxation is recovered. The observation of a stretched-exponential decay is generally associated with the presence of a distribution of relaxation times, the smaller β, the broader the distribution. In general, this distribution has no physical meaning; however, a stretched exponential-function can be the analytical results of a limiting behavior, as, for example, in the case of the single-particle dynamics of hydrogen atoms on a polymer whose thermal motion is described by the Rouse model. This is a consequence of the fact that the mean-square displacement scales in time as $t^{1/2}$.[52]

The agreement between the calculated MIDAS response and the analytical expectation is very good. However, it is noticeable that in the case of the stretched exponential-functions, MIDAS overestimates the normalized ISF at short times. This effect is visible for $\beta = 0.7$ but is much more pronounced for $\beta = 0.5$.[53] Two possible factors could cause this discrepancy. First, the incoming beam-modulation can be approximated with a cosine function only within a limited range and, as larger values of ΔE are probed, which corresponds to shorter time scales, the approximation in Eq. (8) becomes less accurate. Second, the presence of the NVS Gaussian envelope introduces a similar deformation of the cosine. To estimate this latter contribution, we investigate the effect of changing the NVS $\Delta\lambda/\lambda$ on the MIDAS response on a spectrum, which is the Fourier transform of a stretched exponential with $\beta = 0.5$.

Figure 4 shows that as the Gaussian envelope of the incoming beam gets broader the agreement between the theoretical function and the MIDAS response improves significantly, although some discrepancy can be still discerned. This result (also in view of the good agreement between MIDAS and the theoretical calculation for Lorentzian functions as broad as 0.2 meV FWHM shown in Fig. 2) indicates that the discrepancies originate from the very broad components of the stretched exponential and not from an intrinsic deficiency of MIDAS in this time range.

So far, we have assumed that the phase of the incoming-beam modulation can be controlled to have a maximum or a minimum matching the energy selected using the crystal analyzer. As mentioned above, this should be possible either by the use of a phase coil or by setting up the $\pi/2$ flippers. On the other hand, it is common practice in the operation of NSE spectrometers to scan the phase to determine the echo in the scattered beam. In NSE spectrometers, the phase corresponds to the difference in field integral experienced by the neutrons in the first and second arms of the detector. Such a

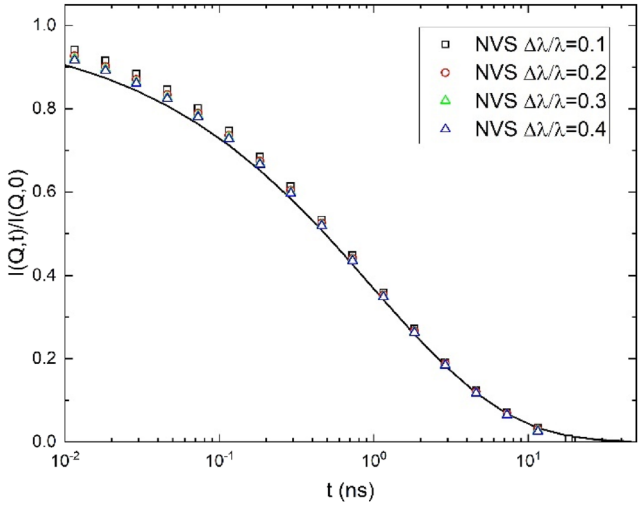

FIG. 4. Normalized ISF calculated as the response of MIDAS as detailed in the text for the Fourier transform of a stretched exponential-function with characteristic time 1 ns and stretching exponent 0.5. The symbols correspond to different values of the FWHM of the Gaussian envelope of the incoming beam. The continuous lines represent the corresponding analytical normalized ISFs.

difference is exquisitely sensitive to magnetic environmental disturbances of the order of the mGauss (10^{-7} T) and can be also affected by changes in the sample shape. In NSE, the phase is scanned using a coil located in only one of the arms. If the accuracy with which the incoming beam modulation is determined was not satisfactory, a scan of the phase can be envisioned for MIDAS as well. From Eq. (9), we define $\phi_0 + \gamma\sqrt{\frac{m_n}{2E_f}}J - 2n\pi = \phi + \theta$, where, now, θ represents the offset between the nominal and experimentally observed phase, and ϕ is, instead, a phase term, which can be controlled by manipulating either the $\pi/2$ flippers or the field integral. Considering that $S(Q, \Delta E)$ is an even function, calculating the cosine of the sum, the detected intensity as a function of ϕ results in a cosine-like modulation around a value proportional to the average scattering intensity, A_v, whose amplitude, around $\phi + \theta = 0$, normalized to the average, A_{mp}, is given by $\frac{I(Q,t_F)}{I(Q,0)}$,

$$N_d(\phi) = A_v[1 + A_{mp}\cos(\phi + \theta)]. \tag{29}$$

To validate this, we consider the simplest scan method commonly employed on the NSEs at ILL—a four-point scan with the phase, ϕ, spaced by $\pi/2$. The results are reported in Fig. 5. The values of the four measured intensities are

$$E_1 = N_d(0) = A_v[1 + A_{mp}\cos\theta],$$

$$E_2 = N_d(\pi/2) = A_v[1 - A_{mp}\sin\theta],$$

$$E_3 = N_d(\pi) = A_v[1 - A_{mp}\cos\theta],$$

$$E_4 = N_d(3\pi/2) = A_v[1 + A_{mp}\sin\theta], \tag{30}$$

which give

$$A_v = \frac{E_1 + E_2 + E_3 + E_4}{4},$$

$$\theta = tan^{-1}\frac{E_4 - E_2}{E_1 - E_3},$$

$$A_{mp} = 2\frac{\sqrt{(E_1 - E_3)^2 + (E_4 - E_2)^2}}{E_1 + E_2 + E_3 + E_4}. \quad (31)$$

In this operation mode, the normalized ISF after normalization for the instrumental resolution function is

$$\frac{I(Q, t_F)}{I(Q, 0)} = \frac{A^s_{mp}(J)}{A^R_{mp}(J)}, \quad (32)$$

where, as in Eq. (23), the superscripts s and R indicate that the counts have been taken on the sample or the resolution.

Figure 5 demonstrates the agreement between the calculated results and the modeling using Eq. (30).

It should be noticed, however, that since in MIDAS, the precession takes place only in the first arm, its phase should be less dependent on the details of the experimental conditions than in NSE. Moreover, it could be envisioned that the first arm of MIDAS be contained in a μ-metal box that would make it less sensitive to external magnetic disturbances.[54]

As mentioned above, the visibility of the incoming beam-modulation that affects MIDAS resolution will depend on the field-integral inhomogeneities. A precise calculation of this requires detailed modeling and depends critically on the design of the instrument. The beam size, length of the precession areas, divergence of the beam, etc., would affect the design and performance of the primary spectrometer. Such a detailed study is beyond the scope of the present paper. However, it is important to provide the reader with some reference points. To the best of our knowledge, MIEZE spectrometers match their resolution to the limitation imposed by ToF on sample geometry and scattering angle (some recent developments notwithstanding[49]) and, therefore, do not usually extend far beyond the nanosecond range.[48] Therefore, we will refer here to studies of traditional NSE spectrometers.[3,39] However, it should be kept in mind that in traditional NSE, the field-integral inhomogeneities refer to the path in both the second and first arms and consider detector areas of hundreds of square centimeters. The beam size of MIDAS would likely be similar to that of typical BS spectrometers, which is ≈3 × 3 cm^2. On the other hand, the addition of a polarization analyzer before the sample might degrade the polarization of the beam. Nevertheless, state of the art precession coils are characterized by intrinsic magnetic-inhomogeneities of ~300 ppm.[22] Furthermore, correction elements have been developed that can decrease further this level by a factor of 100. Thus, state of the art NSE spectrometers have magnetic-field inhomogeneities of few ppm, over detector areas[55] of 10 × 10 cm^2.[21,22] To calculate the effect of the field-integral inhomogeneities on MIDAS, the instrument resolution was calculated considering a Gaussian distribution of incoming wavelengths centered at the nominal field-integral value and various values of FWHM, $\Delta J/J$, in the range from 1000 ppm to 1 ppm. The results are reported in Fig. 6. The level of inhomogeneities required not to degrade the crystal-analyzer resolution varies. Strained Si (111), polished Si (111), and GaAs (200) crystal analyzers would require $\Delta J/J$ of the order of 100, 20, and 5 ppm, respectively. Since the time scale-limit is determined using the crystal analyzer, the trade-off between field-integral homogeneity and beam intensity would be a main design factor.

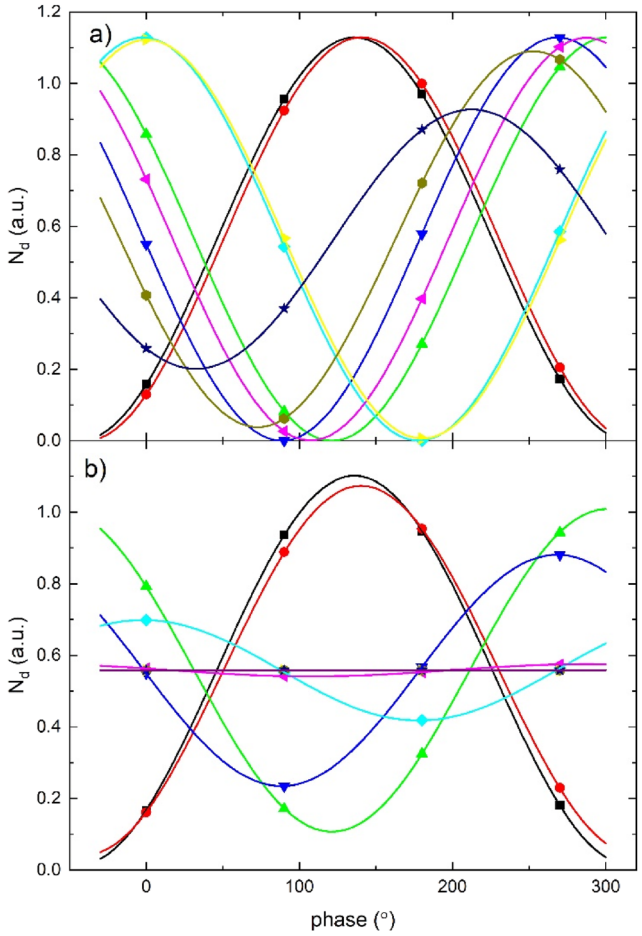

FIG. 5. Modulation of the intensity detected by MIDAS with Si (111) analyzers as a function of phase. Lines are cosine oscillations defined using Eqs. (29) and (31). Plot (a) refers to the resolution, and plot (b) refers to the sample, modeled with a Lorentzian with Γ = 10 μeV. The points and lines of different colors correspond to different values of J and Fourier time (black, red, green, blue, cyan, magenta, yellow, dark yellow, and navy correspond to field integrals of 0.0001, 0.0003, 0.0006, 0.0016, 0.0040, 0.0100, 0.0251, 0.0631, and 0.1585 Tm and Fourier times of 0.0046, 0.0115, 0.0290, 0.0728, 0.1829, 0.4595, 1.1541, 2.8990, and 7.2820 ns).

The neutron flux on the sample in MIDAS is very high because the incoming beam is not highly monochromatized. However, MIDAS is not based on an echo concept, and therefore, only a small fraction of the neutrons impinging on the sample is detected. Nevertheless, the information content on the dynamic structure factor is encoded in the amplitude of the modulation of ρ_2 and is, therefore,

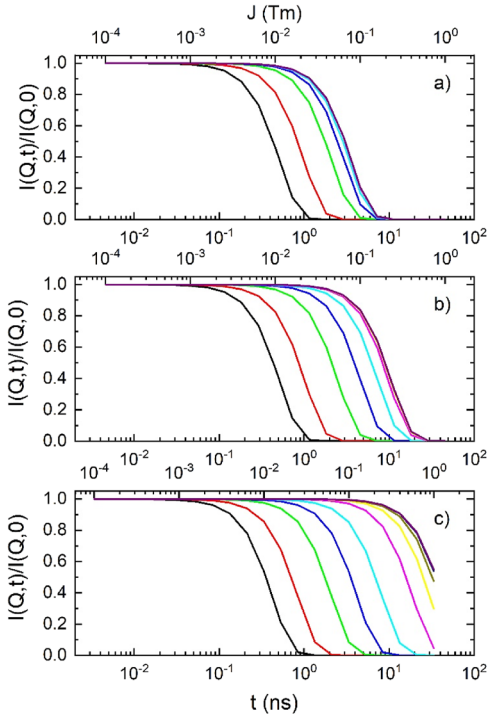

FIG. 6. Effect of field-integral inhomogeneities on MIDAS resolution. $\Delta J/J$ = 1000 ppm (black), 500 ppm (red), 200 ppm (green), 100 ppm (blue), 50 ppm (cyan), 20 ppm (magenta), 10 ppm (yellow), 5 ppm (dark yellow), 2 ppm (navy), 1 ppm (purple). Plots (a), (b), and (c) refer to strained Si (111), polished Si (111), and GaAs (200) crystal analyzers, respectively.

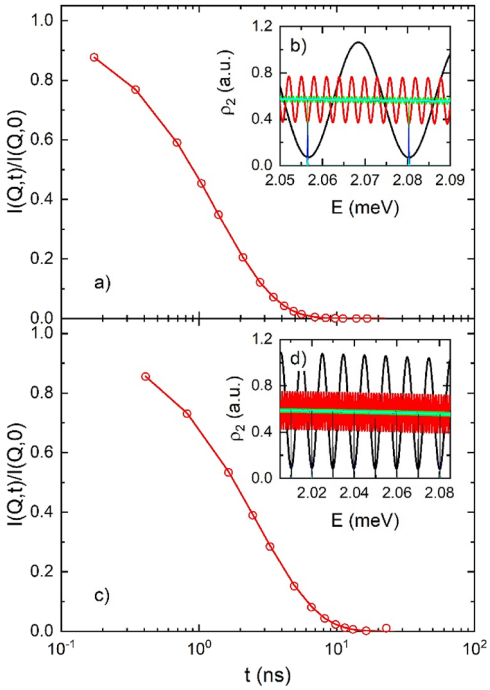

FIG. 7. Calculated response of MIDAS with the multi-analyzer option. Plot (a) refers to the case of a Si (111) and CaF_2 (111) analyzer couple. Plot (b) displays the calculated scattered neutron-energy distribution for different values of the field integral (black, red, green, blue, and cyan lines correspond to field integral values of 0.0037, 0.0300, 0.0899, 0.1799, and 0.3598 Tm and Fourier times of 0.2, 1.4, 4.2, 8.3, and 16.7 ns); the shaded areas around E = 2.0803 meV and E = 2.0565 meV represent the neutrons selected using the Si (111) and CaF2 (111) analyzers, respectively. Plot (c) refers to the case of a series of CaF_2 (111) crystals at different temperatures between 80 and 700 K; plot (d) displays the calculated scattered neutron-energy distribution for three values of the field integral (black, red, green, blue, and cyan lines correspond to field integral values of 0.0088, 0.0702, 0.2106, 0.4211, and 0.8423 Tm and Fourier times of 0.4, 3.2, 9.8, 19.7, and 39.4 ns), and the shaded areas represent the neutrons selected using the analyzers at different temperatures.

spread out in the whole energy range. Since the choice of E_f is arbitrary, the information on the dynamic structure factor is contained in all the peaks (or valleys). The spread in E_f values would be at most as large as that of the incoming wavelength distribution function set using the NVS, which will define the uncertainty in Q. This affords the possibility to employ multiple backscattering analyzers simultaneously to improve the counting rates. All the analyzers, one behind the other, would reflect the neutrons to the same detector, where the signal would be summed up. Although the information on the detected neutron-energy is lost, the modulation information is retained, so the ISF can still be obtained. The multiple analyzers should be such that for all selected wavelengths, λ_f^i, Eq. (13) or Eq. (20) is satisfied; this implies that $\lambda_f^i - \lambda_f^{i+1}$ is constant; moreover, the minimum field-integral will be defined as

$$J_{\min} = \frac{2\pi h}{\gamma m_n} \frac{1}{\left(\lambda_f^i - \lambda_f^{i+1}\right)}. \tag{33}$$

All other field integrals should be even multiples of $J_{\min}$,

$$J = 2iJ_{\min}. \tag{34}$$

For example, we could imagine employing two analyzers Si (111) and CaF_2 (111). Both crystals have been used in modern backscattering spectrometers and are available in large quantities because of their use in the semiconductor industry. The reflected wavelengths are the same within 1%: $\lambda_f^{CaF_2(111)}$ = 6.3070 Å and $E_f^{CaF_2(111)}$ = 2.0565 meV, whereas $\lambda_f^{Si(111)}$ = 6.2708 Å and $E_f^{Si(111)}$ = 2.0803 meV, which result in $J_{\min}$ = 0.0037 Tm. Moreover, they provide similar energy resolutions, ≈0.06 and ≈0.08 μeV, respectively.[2] This is exemplified in Figs. 7(a) and 7(b). The normalized ISF is still measured accurately. On the other hand, the minimum Fourier time is of the order of ≈0.1 ns. The same approach could be extended to a larger number of analyzers. The temperature dependence of the lattice spacing in CaF_2 over the range from 80 to 700 K is already used to scan the incoming energy from 2.0803 to 2.0103 meV on IN13.[42,43] It is conceivable that a series of aligned CaF_2 crystals at different temperatures (say eight) could be used. This is illustrated in Figures 7(c) and 7(d). Other possible ways to realize a suitable array of crystals would rely on crystal-doping, as, for example, silicon/germanium, as envisaged for the spectrometer MUSICAL.[56]

IV. COMPARISON OF MIDAS AND BACKSCATTERING VIA MONTE CARLO SIMULATION

In simple terms, MIDAS accepts many more neutrons from the source than BS, but the losses are greater due to the polarization, flippers, and precession regions. There is also the question of how the extra neutrons may contribute to the background, which would mainly affect the possible use of MIDAS for inelastic scattering. The central question for this simulation is whether MIDAS is worthwhile, that is, can it at least match the performance of a backscattering instrument over the same dynamic range? Comparison of instruments that operate on different principles is always difficult because their attributes rarely match, and in the current comparison, the measurements are also in different domains. BS measures in the energy domain, while MIDAS measures in the time domain, and unfortunately, there is no straightforward way of passing statistical errors through the Fourier transform that relates these domains. We overcome this difficulty by using the same number of incident neutrons to generate the same number of spectral data-points in each domain (time for MIDAS and energy for BS). We then compare the errors of the two methods, with particular reference to the sensitivity of the methods to the sample function.

Because we are not designing practical instruments, and we need only consider a single scattering angle, we can strip both techniques down to the bare minimum components. We accept that additional focusing and phase-space transformations may alter the relative merits of the instrumental setups that we use here, so our question is the following: how the two techniques compare, each in its most basic form?

There are two crucial differences between wavelength-selecting elements in a real instrument and a simulated instrument. First, simulation detectors can have excellent neutron-energy analysis, while real detectors have no practical energy-analysis. Second, in a simulation, the source itself can be defined to produce a very narrow wavelength band, centered at some desired wavelength, while real sources require monochromators to prepare the incident neutron beam. Because the objective is only to compare the fundamentals of MIDAS and BS, we use these simulation-advantages to make the instruments as simple and comparable as possible, accepting that both are fictive. These simulated instruments are shown in Fig. 8, which for BS consists only of a source, a guide, a sample, and a detector.

A. The source and guide

The schematic illustrations of the BS and MIDAS instruments are shown in Fig. 8. A 5.0 cm high by 4.0 cm wide source with 1° (FWHM) horizontal and vertical divergence was selected with an entrance slit of the same size to a 29.5 m natural nickel-coated guide.

The parallel guide was also 5 cm high by 4 cm wide. No velocity selector was used because the wavelength bandwidth of the source can be selected to suit MIDAS or BS (see above). For MIDAS, this was selected to be centered at 6.271 Å with a full width of 0.1 Å to ensure full coverage of the energy range. The BS instrument was rather different because the source was used to emulate the Doppler monochromator, which gives the BS instrument a false advantage (100% efficiency of the monochromator) but enables the simulated BS and MIDAS instruments to be much more similar. For the BS instrument, the wavelength bandwidth from the source was always 0.0004 Å half-width, corresponding to a full-width energy-resolution of 0.53 μeV. This was centered at different wavelengths to produce the energy-shifts relative to the analyzer crystals that would normally be produced by the velocity of the Doppler monochromator. Clearly, with the wavelength band centered at 6.271 Å, the energy-transfer is zero.

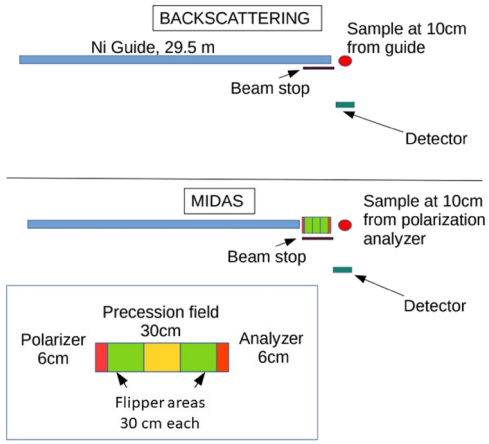

FIG. 8. Schematic illustration of the BS and MIDAS as modeled in the McStas simulation.

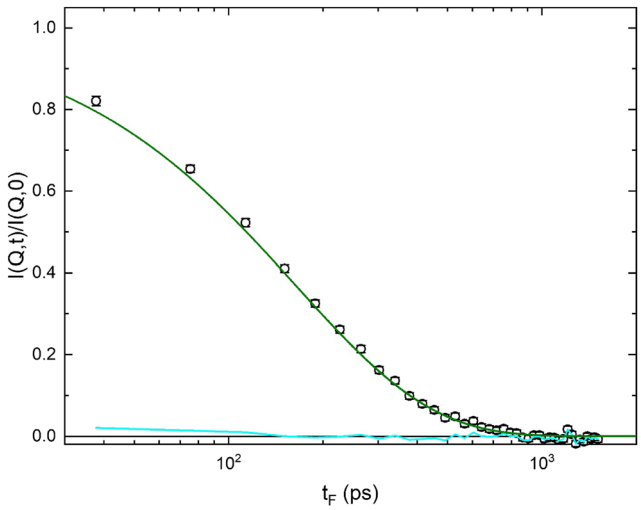

FIG. 9. ISF as measured by MIDAS in the McStas simulation. Data points are the obtained counts. The continuous green line is the calculated Fourier transform of the simulated dynamics structure factor, a Lorentzian with FWHM of 4 μeV. The cyan line is the difference between the obtained counts and the theoretical calculation. Error bars represent one standard deviation.

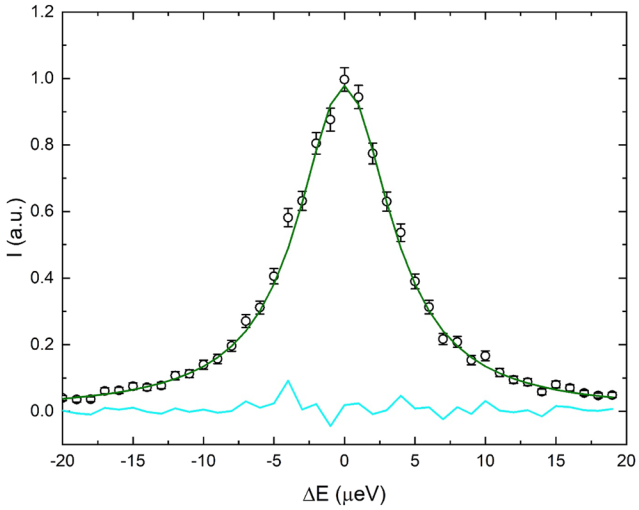

FIG. 10. Dynamic structure factor convoluted with the instrumental resolution function as measured using the BS instrument in the McStas simulation. Data points are the obtained counts. The continuous green line is the Lorentzian with FWHM of 4 μeV. The cyan line is the difference between the obtained counts and the Lorentzian function. Error bars represent one standard deviation.

B. Primary spectrometer

For BS, the guide leads directly to the sample with a 10 cm gap before the sample to allow for some sample environment. For MIDAS, the primary spectrometer is at the end of the 29.5 m guide. The only important aspect of the primary spectrometer is its length because this determines the neutron loss due to the absence of a guide. Nevertheless, we have chosen practical dimensions for each element, even though it is only the total length that is of concern. Because we are using typical BS resolution, not NSE, the field integral is smaller than in normal NSE. The first and last elements are the polarizer and analyzer, each of which is 6.0 cm long. Both elements are algorithms that artificially align and analyze neutron spins. The two $\pi/2$ flippers each occupy a region 30 cm long, although, in practice, the device is rather thin. The total length of the primary spectrometer is 102 cm. To quantify the loss due to these components, a simple McStas simulation showed that the 100 cm gap between the guide-end and the sample reduces the flux by 19%. This is followed by a 10.0 cm gap to the samples, analogous to the BS.

C. Sample

A simple annular sample shape, with 5 cm height, 2 cm radius, and 5 mm thickness, was used, for which the width of quasi-elastic broadening could be assigned. A "vanadium-option" is provided by McStas, which allows a delta function for the sample, corresponding to the usual vanadium-sample.

D. Secondary spectrometer

In simple terms, the secondary spectrometer for both BS and MIDAS can be made identical so that the only practical difference between MIDAS and BS is the polarization and analysis segment of the MIDAS primary spectrometer. As alluded to above, simulation detectors can have excellent neutron-energy analysis so that we can eliminate the backscattering analyzer and make the energy analysis directly at the detector. The resulting secondary spectrometer has only a single component—a detector, from which neutrons with wavelengths between 6.2706 and 6.2714 Å (energy-resolution of 0.53 μeV) were accumulated. The combined primary and secondary resolution was 0.75 μeV. Furthermore, we need only place a single detector at a convenient position with respect to the sample. A beam-stop is included alongside the end of the guide as a precaution to any spurious scattering from the primary spectrometer.

V. RESULTS

In all comparisons below, the MIDAS flux was reduced by a factor of 2 to take account of the polarization. For BS, the data collection consisted of selecting 40 wavelengths at the source corresponding to equally spaced energy-transfers, ΔE, between -20 μeV and $+20$ μeV, with $\Delta E = 0$ for $\lambda = 6.27$ Å. Each point was collected for a preset number of neutrons as defined by McStas, resulting in a simulated BS energy spectrum. For MIDAS, the time scan contained the same number of points as BS and was made by varying the precession-field such that the number of spin-precessions, N, varied from 38.5 to 1558.5, in 40 steps of 38 in N, covering a time range corresponding to the same total energy-range as the BS spectrum. The integer+0.5 turns ensures that Eq. (20) is satisfied.

The sample function was Lorentzian with $\Gamma = 4$ μeV (HWHM) corresponding to a relaxation time of 164.4 ps, which is fairly typical of samples studied with BS. The McStas "ncount" parameter defines the total number of neutrons from the source, regardless of the width of the wavelength band chosen. Consequently, the flux at a given wavelength reduces in proportion to the width of the wavelength band. In a real source, the flux would be essentially constant at all wavelengths within the ranges considered here. Because the BS source bandwidth was 0.0004 Å (square) and the MIDAS bandwidth was 0.1 Å (square), there is a factor of 250 for the flux at a given wavelength between the sources for the two instruments. This was taken into account in selecting the "ncount" parameter. The input sample functions for MIDAS and BS are compared with the outpuf of the McStas simulations in Figs. 9 and 10, respectively.

A simple comparison of the total number of counts at the detector for the two instruments shows that MIDAS has 78-times more counts in the above experiment. This apparent advantage arises from the much larger wavelength bandwidth from the source for MIDAS compared with the tightly monochromated incident resolution function of BS. This is directly analogous to part of the count-rate advantage of NSE, where the key question is how much of this advantage is lost when signal-to-noise ratio is taken into account. The overall gain or loss can conveniently be assessed by mimicking the data analysis via fitting the spectra against a presumed input sample-function (Lorentzian in this case).

A. Data treatment and fitting

To emulate a real experiment, the resolution function was measured using the McStas "vanadium sample" (a pseudo-delta-function) for both instruments. Sample and vanadium spectra

TABLE I. Results of the fitting (mixed method, no derivatives) of the McStas results.

	Γ (HWHM) ps (μeV)	Err	Err/value
MIDAS	164.6	4.82	0.029
BS width	161.7 (4.07)	10.67	0.066
BS intensity	12.3	0.61	0.050
	Input 164.5		

for BS were used in fitting without further treatment. Because MIDAS was run in the integer+0.5 mode [Eq. (20)], the measured function is

$$a - a * f,$$

where f is the sample function and a is a scalar that can be obtained by running the experiment for a short time with the flippers switched off. For MIDAS, the resolution correction is made by simply dividing the measured sample curve by the vanadium curve. The result can either be fitted using "a" as a fixed-value parameter or transformed to the sample function, f, before fitting. There is no real difference between these alternatives, but we prefer the latter because this function is more familiar.

Fitting of MIDAS and BS data was made using locally written routines. For BS, the trial functions in the minimization routine were numerically convoluted with the measured resolution function to provide the fitted function. This function was compared with the measured function to obtain a difference function. The procedure was repeated iteratively by adjusting the parameters to minimize the difference function. The use of a numerical convolution is preferable to a Fourier transform method, but the derivatives are obtained by finite differences rather than analytically. The algorithm to obtain estimated errors on the parameters uses finite differences to obtain the correlation matrix, with the standard errors being taken from the diagonal of the variance–covariance matrix. With only 1 parameter for fitting MIDAS data, and 2 for BS, the error procedure is trivial. The results of the fitting are summarized in Table I.

The input sample function was a Lorentzian with Γ = 4.0 μeV (HWHM), which is to be compared with the BS fitted value of 4.07 μeV. In the time domain, these correspond to Γ of 164.4 and 161.7 ps, respectively, giving a difference of 2.7 ps, which is well inside the estimated error of 10.67 ps. The value of this error is important because it shows the sensitivity of the fit to changes in the parameter. For BS, the overall scalar, or intensity, also has to be fitted and the relative error of the intensity (0.050) is similar to that of the relaxation time (0.066).

For MIDAS, the agreement between the input and fitted T is remarkably good. Although such close agreement may be fortuitous, the important factor is the estimated error, which is less than half the corresponding error for BS. Interestingly, this shows that not only does MIDAS produce a more accurate result but is also more sensitive to changes in the sample function. At least some of this sensitivity is because MIDAS requires only a single parameter to fit this sample function, whereas BS requires two. In practice, for BS, it is generally very hard to determine with confidence and satisfactory accuracy the total spectral intensity, whereas MIDAS can determine this experimentally in a satisfactory way by turning off the π/2 flippers.

VI. DISCUSSION AND REMARKS FOR THE FUTURE

In this section, we will discuss how MIDAS compares with other established methods and instruments for measuring dynamics using neutrons.

As mentioned above, MIDAS represents a FTNS method. Hence, it allows for a high count rate because the whole spectrum is measured at once. However, this is obtained at the expense of a poorer signal-to-noise ratio (defined for MIDAS as the ratio between the amplitude and the average of the modulation). Such a trade-off is certainly problematic for the study of inelastic features but is not significantly detrimental for relaxation phenomena where the information is contained in the width of the elastic line.

Other NSE methods, such as MIEZE or RNSE, as well as TOFLAR (Time Of Flight and LARmor precession technique),[57] have historically been limited in the time scale accessible, usually being smaller than one nanosecond. Recent developments have led to the possibility to overcome these limitations. However, these methods would not allow for a large scattering angle coverage.[48,49]

In Secs. IV and V, we have carried out a comparison between MIDAS and a basic backscattering spectrometer. The results indicate that the two instruments would result in comparable data acquisition efficiency, with MIDAS providing, within the conditions tested, a factor of 2 smaller error bars in the determination of the sample characteristic relaxation time. To a first approximation for a QENS experiment, the count rate of a backscattering machine scales roughly with the inverse square of the instrumental energy resolution because for an optimized instrument, both energy monochromator and analyzer need to narrow their resolution. For MIDAS, improving the analyzer by a factor of 2 would only linearly decrease the data acquisition rate because no adjustment to the primary spectrometer that affects the flux would be needed, to a first approximation. Therefore, the improved accuracy of MIDAS in the sample relaxation rate determination should increase with the resolution.

Unlike NSE, the primary spectrometer of MIDAS is decoupled from the secondary spectrometer so that any means of producing a modulated beam would suffice, and it is conceivable that a suitable chopper system would enable the FTNS principle to be used at a pulsed source. However, in its present concept, MIDAS is a continuous source instrument. As compared to the current state of the art backscattering spectrometers, it will allow for a larger dynamic range extending to the picosecond region, which corresponds to energy transfers of the order of hundreds of μeV. This constraint on the dynamic window at a continuous source has only been addressed by the BATS mode on IN16B, and a comparison is not straightforward.[5] On the other hand, state-of-the-art backscattering spectrometers employ Phase Space Transformation (PST) choppers, which can increase the flux at the sample by a factor of ≈5.[10] An interesting comparison to estimate the effect of the guide to sample setup and distance could be carried out by looking at the backscattering and NSE instruments at the NCNR. The monochromatic (≈0.8 μeV) flux at the sample on HFBS was measured as 2.5 10^5 n/cm^2/s (a recent increase in flux on HFBS was achieved using a recently developed

focusing guide). For the NSE, with $\Delta\lambda/\lambda \approx 20\%$, the flux at the end of the guide is 1.08 10^8 n/cm^2/s, whereas at the sample, it is 2.7 10^7 n/cm^2/s. This translates to a corresponding monochromatic flux of $\approx$2 10^5 and $\approx$5 10^4 n/cm^2/s. For the NGA-NSE, the guide to sample distance is 2.5 m, optimized to measure Fourier times up to 20 ns using 6 Å. Therefore, this comparison suggests that, as hinted before, if a shorter guide to sample distance could be designed to achieve the relevant time scales, the flux on MIDAS and a corresponding backscattering instrument would be similar at a specific wavelength, apart for the loss due to polarization, even considering the effect of a PST.

On the one hand, MIDAS is not an echo method as no decoding or refocusing is carried out in the second arm. This implies that, although the flux at the sample is comparable to that of a NSE spectrometer, the detection rate is not as high. On the other, the fact that the scattered beam does not need refocusing and, therefore, manipulation of the neutron spins allows the angular range covered using the detectors to be increased. To a first approximation, Fig. 6 indicates that an accessible time scale similar to those available on WASP for the same wavelength could be obtained using strained analyzer crystals. Although we make no instrument simulation for comparing MIDAS with WASP, we can make some general estimates. The gain in data acquisition rate from the echo can be estimated as the ratio between the wavelength spread at the sample, here defined by the velocity selector, and the wavelength spread defined using the analyzer. This ratio is of the order of 0.2/(0.6/2080) $\approx$ 700. In order to estimate the gain from a larger scattering angle coverage, we compare the vertical coverage of WASP, which is of the order of 2.5°, with those of BASIS at SNS or DNA at MLF, which are of $\approx$40.[12,13] Therefore, WASP should have a higher data acquisition rate than MIDAS by a factor of $\approx$40. However, an important parameter less straightforward to estimate is the distance between the guide and the sample, which depends on the beam technical details and which could be possibly made more compact utilizing state of the art optimally shaped precession coils and correction coils on MIDAS than the large Helmholtz coils employed by WASP.

Data acquisition rates on MIDAS could be significantly enhanced using multiple analyzers. This possibility is within the current trend of neutron instruments at continuous sources, which employ an analyzer array for multiplexing of data acquisition. Such concepts are employed on the reflectometer CANDOR at the NCNR and on the triple axis CAMEA at SINQ. The Fourier transform concept of multiplexing envisioned for MIDAS is advantageous in the high resolution limit for quasielastic measurement. It is not efficient for the study of large energy transfers where covering different exchanged energy regions at the same time is possible and better matches the scientific need to explore a broad dynamic range efficiently. The MIDAS concept is valuable where the information is contained in a region of energy exchanges centered around zero. In the multiplexing option, the need to maintain a dynamic window of at least one order of magnitude, a reasonable ratio between the analyzer resolutions, their number, and energy spacing implies that highly monochromatizing analyzer crystals should be used.

In conclusion, MIDAS offers new possibilities to optimize the dynamic range and data acquisition rate in neutron spectrometers, overlapping the current ranges of BS and NSE. If a practical realization of the multi-analyzer concept could be implemented, a significant increase in the data acquisition rate or corresponding extension of the dynamic window of backscattering spectrometers would be possible.

ACKNOWLEDGMENTS

The authors are indebted to Drs. Bela Farago and Markus Appel from ILL and Drs. Leland Harriger and Madhusudan Tyagi from NCNR for critical reading of the manuscript. The authors also thank Dr. Richard Lindstrom for performing the gold foil measurements of the neutron flux for the NSE spectrometer at the NCNR. The authors acknowledge the support from the University College Dublin (UCD) under the Seed Funding Scheme (Grant No. SF2008), with additional support provided by UCD School of Physics.

Certain commercial equipment, instruments, or materials (or suppliers, software, etc.) are identified in this paper to foster understanding. Such an identification does not imply recommendation or endorsement by the National Institute of Standards and Technology, nor does it imply that the materials or equipment identified are necessarily the best available for the purpose.

AUTHOR DECLARATIONS

Conflict of Interest

The authors have no conflicts to disclose.

Author Contributions

Antonio Benedetto: Conceptualization (equal); Formal analysis (equal); Writing – original draft (equal); Writing – review & editing (equal). **Gordon J. Kearley**: Conceptualization (equal); Formal analysis (equal); Writing – original draft (equal); Writing – review & editing (equal). **Antonio Faraone**: Conceptualization (equal); Formal analysis (equal); Writing – original draft (equal); Writing – review & editing (equal).

DATA AVAILABILITY

The data that support the findings of this study are available from the corresponding author upon reasonable request.

REFERENCES

[1] J. S. Gardner, G. Ehlers, A. Faraone, and V. García Sakai, Nat. Rev. Phys. **2**(2), 103–116 (2020).
[2] B. Frick and D. Neumann, in *Neutrons in Soft Matter* (2011), pp. 183–202.
[3] F. Mezei, in *Lecture Notes in Physics*, edited by F. Mezei, C. Pappas and T. Gutberlet (2003), Vol. 601, pp. 5–14.
[4] M. Appel and B. Frick, Rev. Sci. Instrum. **88**(3), 036105 (2017).
[5] M. Appel, B. Frick, and A. Magerl, Physica B **562**, 6–8 (2019).
[6] B. Frick and M. Appel, Acta Crystallogr., Sect. A: Found. Adv. **72**, S294 (2016).
[7] B. Frick, J. Combet, and L. van Eijck, Nucl. Instrum. Methods Phys. Res., Sect. A **669**, 7–13 (2012).
[8] J. Wuttke, A. Budwig, M. Drochner, H. Kämmerling, F.-J. Kayser, H. Kleines, V. Ossovyi, L. C. Pardo, M. Prager, D. Richter, G. J. Schneider, H. Schneider, and S. Staringer, Rev. Sci. Instrum. **83**(7), 075109 (2012).
[9] N. R. de Souza, A. Klapproth, and G. N. Iles, Neutron News **27**(2), 20–21 (2016).

[10]A. Meyer, R. M. Dimeo, P. M. Gehring, and D. A. Neumann, Rev. Sci. Instrum. **74**(5), 2759–2777 (2003).
[11]K. Kuhlmann, M. Appel, B. Frick, and A. Magerl, Rev. Sci. Instrum. **90**(1), 015119 (2019).
[12]E. Mamontov and K. W. Herwig, Rev. Sci. Instrum. **82**(8), 085109 (2011).
[13]K. Shibata, N. Takahashi, Y. Kawakita, M. Matsuura, T. Yamada, T. Tominaga, W. Kambara, M. Kobayashi, Y. Inamura, T. Nakatani, K. Nakajima, and M. Arai, J. Phys. Soc. Jpn., in *Proceedings of the 2nd International Symposium on Science at J-PARC — Unlocking the Mysteries of Life, Matter and the Universe* (The Physical Society of Japan, 2015), Vol. 8, pp. 036022.
[14]N. Tsapatsaris, R. E. Lechner, M. Marko, and H. N. Bordallo, Rev. Sci. Instrum. **87**(8), 085118 (2016).
[15]C. J. Carlile and M. A. Adams, Physica B **182**(4), 431–440 (1992).
[16]C. Pappas, G. Kali, P. Boni, R. Kischnik, L. A. Mertens, P. Granz, and F. Mezei, Physica B **276–278**, 162–163 (2000).
[17]C. Pappas, G. Kali, T. Krist, P. Boni, and F. Mezei, Physica B **283**(4), 365–371 (2000).
[18]P. Fouquet, G. Ehlers, B. Farago, C. Pappas, and F. Mezei, J. Neutron Res. **15**, 39–47 (2007).
[19]C. Do, R. Ashkar, C. Boone, W. R. Chen, G. Ehlers, P. Falus, A. Faraone, J. S. Gardner, V. Graves, T. Huegle, R. Katsumata, D. Kent, J. Y. Y. Lin, B. McHargue, B. Olsen, Y. Y. Wang, D. Wilson, and Y. Z, Rev. Sci. Instrum. **93**(7), 075107 (2022).
[20]B. Farago, P. Falus, I. Hoffmann, M. Gradzielski, F. Thomas, and C. Gomez, Neutron News **26**(3), 15–17 (2015).
[21]S. Pasini, O. Holderer, T. Kozielewski, D. Richter, and M. Monkenbusch, Rev. Sci. Instrum. **90**(4), 043107 (2019).
[22]S. Pasini and M. Monkenbusch, Meas. Sci. Technol. **26**(3), 035501 (2015).
[23]M. Ohl, M. Monkenbusch, N. Arend, T. Kozielewski, G. Vehres, C. Tiemann, M. Butzek, H. Soltner, U. Giesen, R. Achten, H. Stelzer, B. Lindenau, A. Budwig, H. Kleines, M. Drochner, P. Kaemmerling, M. Wagener, R. Möller, E. B. Iverson, M. Sharp, and D. Richter, Nucl. Instrum. Methods Phys. Res., Sect. A **696**(Supplement C), 85–99 (2012).
[24]B. Farago, J. Neutron Res. **10**(3–4), 169–171 (2002).
[25]A. V. Skripov, M. Dimitrievska, O. A. Babanova, R. V. Skoryunov, A. V. Soloninin, F. Morelle, Y. Filinchuk, A. Faraone, H. Wu, W. Zhou, and T. J. Udovic, J. Phys. Chem. C **123**(34), 20789–20799 (2019).
[26]T. Keller, H. Trepka, K. Habicht, and B. Keimer, Phys. Status Solidi B **259**(5), 2100164 (2022).
[27]W. G. Bouwman, R. Pynn, and M. T. Rekveldt, Physica B **350**(1–3), E787–E790 (2004).
[28]M. T. Rekveldt, J. Plomp, W. G. Bouwman, W. H. Kraan, S. Grigoriev, and M. Blaauw, Rev. Sci. Instrum. **76**(3), 033901 (2005).
[29]Y. Ito, M. Nishi, and K. Motoya, "Neutron spectral modulation as a new thermal neutron scattering technique I. General theory," Nucl. Instrum. Methods Phys. Res. **198**(2–3), 497–513 (1982).
[30]H. H. Grapengeter, B. Alefeld, and R. Kosfeld, Colloid Polym. Sci. **265**(3), 226–233 (1987).
[31]B. Frick and D. Richter, Science **267**(5206), 1939–1945 (1995).
[32]B. Frick, D. Richter, W. Petry, and U. Buchenau, Z. Phys. B **70**(1), 73–79 (1988).
[33]A. Benedetto and G. J. Kearley, Sci. Rep. **11**(1), 14093 (2021).
[34]A. Benedetto and G. J. Kearley, Sci. Rep. **10**(1), 6350 (2020).
[35]A. Benedetto and G. J. Kearley, Sci. Rep. **9**, 11284 (2019).
[36]A. Benedetto and G. J. Kearley, Sci. Rep. **6**, 34266 (2016).
[37]B. Farago and F. Mezei, Physica B+C **136**(1–3), 100–102 (1986).
[38]C. Pappas, E. Lelievre-Berna, P. Bentley, E. Bourgeat-Lami, E. Moskvin, M. Thomas, S. Grigoriev, and V. Dyadkin, Nucl. Instrum. Methods Phys. Res., Sect. A **592**(3), 420–427 (2008).
[39]P. Dagleish, J. Hayter, and F. Mezei, in *Neutron Spin Echo*, edited by F. Mezei (Springer, 2006), pp. 66–71.
[40]P. K. Willendrup, E. B. Knudsen, E. Klinkby, T. Nielsen, E. Farhi, U. Filges, and K. Lefmann, J. Phys.: Conf. Ser. **528**(1), 012035 (2014).
[41]K. Lefmann, P. K. Willendrup, L. Udby, B. Lebech, K. Mortensen, J. O. Birk, K. KlenØ, E. Knudsen, P. Christiansen, J. Saroun, J. Kulda, U. Filges, M. Konnecke, P. Tregenna-Piggott, J. Peters, K. Lieutenant, G. Zsigmond, P. Bentley, and E. Farhi, J. Neutron Res. **16**, 97–111 (2008).
[42]A. J. C. Dennison, F. Natali, E. Farhi, G. Manzin, P. Courtois, and J. Peters, Nucl. Instrum. Methods Phys. Res., Sect. A **908**, 182–188 (2018).
[43]N. Francesca, J. Peters, D. Russo, S. Barbieri, C. Chiapponi, A. Cupane, A. Deriu, M. Di Bari, E. Farhi, Y. Gerelli *et al.*, Neutron News **19**(4), 14–18 (2008).
[44]T. Krist, F. Rucker, G. Brandl, and R. Georgii, Nucl. Instrum. Methods Phys. Res., Sect. A **698**, 94–97 (2013).
[45]A. Stunault, K. H. Andersen, S. Roux, T. Bigault, K. Ben-Saidane, and H. M. Ronnow, Physica B **385–386**, 1152–1154 (2006).
[46]J. K. Jochum, J. F. K. Cooper, L. M. Vogl, P. Link, O. Soltwedel, P. Boni, C. Pfleiderer, and C. Franz, Quantum Beam Sci. **6**(3), 26 (2022).
[47]T. Oda, M. Hino, M. Kitaguchi, P. Geltenbort, and Y. Kawabata, Rev. Sci. Instrum. **87**(10), 105124 (2016).
[48]C. Franz, O. Soltwedel, C. Fuchs, S. Säubert, F. Haslbeck, A. Wendl, J. K. Jochum, P. Böni, and C. Pfleiderer, Nucl. Instrum. Methods Phys. Res., Sect. A **939**, 22–29 (2019).
[49]R. Dadisman, G. Ehlers, and F. K. Li, Rev. Sci. Instrum. **93**(1), 013301 (2022).
[50]M. Prager and A. Heidemann, Chem. Rev. **97**(8), 2933–2966 (1997).
[51]V. F. Sears, Can. J. Phys. **45**, 237 (1967).
[52]D. Richter, M. Monkenbusch, A. Arbe, and J. Colmenero, *Neutron Spin Echo in Polymer Systems*, 174 (Springer, 2005), pp. 1–221.
[53]In the case of $\beta = 0.5$, the Fourier transform of the stretched exponential-function was calculated as a sum of Lorentzian functions whose distribution was determined as the known analytical Laplace-transform of the stretched exponential, C. P. Lindsey and G. D. Patterson, "Detailed comparison of the Williams–Watts and Cole–Davidson functions," J. Chem. Phys. **73**, 3348–3357 (1980).
[54]E. Mamontov and P. Zolnierczuk, EPJ Web Conf. **272**, 01014 (2022).
[55]The size of the detection area is a relevant parameter for NSE, but it does not apply to MIDAS.
[56]B. Alefeld, Nucl. Instrum. Methods Phys. Res., Sect. A **355**(2–3), 478–483 (1995).
[57]A. Kusmin, L. van Eijck, C. Pappas, P. A. Zolnierczuk, N. Arend, M. Ohl, and A. A. van Well, EPJ Web Conf. **83**, 03009 (2015).